Isoscalar E0, E1, E2, and E3 strength in ^{94}Mo

J. Button, Y.-W. Lui, D. H. Youngblood, X. Chen, G. Bonasera, and S. Shlomo

Phys. Rev. C **94**, 034315 — Published 14 September 2016

DOI: 10.1103/PhysRevC.94.034315

Isoscalar E0, E1, E2, and E3 strength in ^{94}Mo

J. Button[1], Y. -W. Lui[1], D. H. Youngblood[1], X. Chen[2], G. Bonasera[1] and S. Shlomo[1]

[1]Cyclotron Institute, Texas A&M University, College Station, Texas 77843, USA.
[2]Department of Radiation Oncology, Medical College of Wisconsin, Milwaukee, Wisconsin 53226, USA

Isoscalar giant resonances in ^{94}Mo have been studied with inelastic scattering of 240 MeV α particles at small angles including 0°. All of the expected EWSR for the isoscalar E0 resonance was found (112%). A significant portion of the EWSR was found for the isoscalar E1 (83%), E2 (61%), and the high energy octupole E3 (46%) resonances. The strength distributions are compared with the predictions from HF-RPA calculations with the KDE0v1 Skyrme-type interaction.

PACS numbers: 25.55.Ci, 24.30.Cz, 27.60.+j

I. INTRODUCTION

Giant Resonances (GR) are the broad resonances that occur at excitation energies between 10 and 30 MeV. They correspond to the collective motion of nucleons within the nucleus and have modes classified according to their multipolarity L, spin S, and isospin T quantum numbers. The Isoscalar Giant Monopole Resonance (ISGMR) is interesting because its excitation energy is directly related to the incompressibility of the nucleus K_A (1), where $\langle r^2 \rangle$ is the mean square radius and *m* is the mass of the nucleus [1,2].

$$E_{GMR} = \sqrt{\left(\frac{\hbar^2 K_A}{m\langle r^2 \rangle}\right)} \qquad (1)$$

K_A can be used to obtain the incompressibility of nuclear matter K_{NM} by comparison to calculations using mean fields, where the value for K_{NM} is deduced from the interaction that best reproduces the experimental data on the strength functions of the giant resonance. At present, the best value for K_{NM} is 240±20 MeV [3].

Isoscalar giant resonances in the Mo isotopes were first observed by Moalem *et al*. who identified the Giant Quadrupole Resonance (GQR) in all stable Mo isotopes using inelastic scattering of 110 MeV ^{3}He [4]. Duhamel *et al.* [5] investigated the GQR and GMR in ^{92}Mo using inelastic scattering of 152 MeV α particles. Youngblood *et al.* studied the isoscalar giant resonances in ^{90,92,94}Zr and ^{92,96,98,100}Mo [6--8] using inelastic scattering of 240 MeV α particles at small angles including 0°. Ref. [6] focused on the E0 strength distribution, which showed high and low-energy components separated by 7-9 MeV in these Zr and Mo isotopes. The higher energy second peak is not predicted by the HF-RPA calculations that reproduce the ISGMR energies in the other nuclei. For the nuclei with $A \neq 92$, 80-90% of the strength is in the lower energy peak located at 15.7 to 17.2 MeV. In the $A = 92$ nuclei, there is considerably more strength in the higher energy peak than in the higher energy peak of the $A \neq 92$ nuclei. This enhancement of the strength in the higher energy region for ^{92}Zr and ^{92}Mo results in K_A values for these two nuclei that are 8σ and 4σ above those obtained with interactions that predict K_A values in agreement with those for the other Zr and Mo isotopes [6]. The excellent peak-to-continuum ratio [9--12] of data obtained with 240 MeV α particles allows identification of the GDR, GQR, and High Energy Octupole Resonance (HEOR) strength distributions in the range $9 \leq E_x \leq 36$ MeV. The strength distributions for these resonances in the Zr [8] and Mo [7] isotopes

were investigated and compared to the results of spherical Hartree-Fock – based random-phase-approximation (HF-RPA) calculations [13] with KDE0v1 Skyrme-type effective interaction [14].

In this paper we report E0, E1, E2, and E3 multipole strength distributions obtained for ^{94}Mo and compare them to HF-RPA calculations with the KDE0v1Skyrme-type interaction.

II. EXPERIMENTAL PROCEDURE

The experimental technique has been described thoroughly in Refs. [9,10] and is summarized briefly below. Beams of 240 MeV α particles from the Texas A&M K500 super-conducting cyclotron bombarded a self-supporting ^{94}Mo foil of 4.8 mg/cm^2 enriched to more than 95% in the desired isotope, located in the target chamber of the multipole-dipole-multipole spectrometer. The horizontal and vertical acceptance of the spectrometer was 4°. Ray tracing was used to reconstruct the scattering angle. The vertical acceptance was ±2°. The focal plane detector measured position and angle in the scattering plane, covering $E_x \approx$ 8 MeV to $E_x >$ 55 MeV (depending on scattering angle). The out-of-plane scattering angle was not measured. Position resolution of approximately 0.9 mm and scattering angle resolution of about 0.09° were obtained. Cross sections were obtained from the charge collected, target thickness, dead time, and known solid angle. The target thicknesses were measured by weighing and checked by measuring the energy loss of the 240 MeV α beam in each target. The cumulative uncertainties in target thickness, solid angle, etc., result in about a ±10% uncertainty in absolute cross sections. ^{24}Mg spectra were taken before and after each run, and the 13.85±.02 MeV L=0 state [15] was used as a check on the calibration in the giant resonance region.

Data were taken with the spectrometer at 0.0° (0.0° < θ < 2.0°) and at 4.0° (2.0° < θ < 6.0°). Sample spectra obtained for ^{94}Mo are shown in Figure 1.

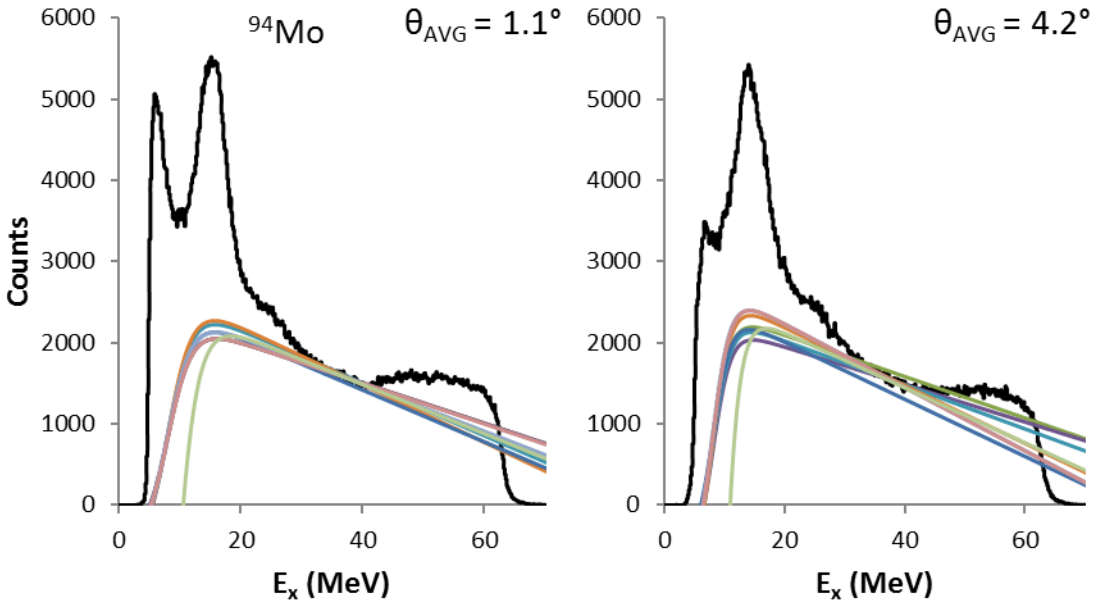

FIG. 1. Inelastic α spectra obtained for ^{94}Mo are shown. The lines are examples of continua chosen for analyses. The bump in the spectra between 45 and 60 MeV is due to (α,5Li) and (α,5He) reactions with subsequent decay into α particle and a nucleon.

III. MULTIPOLE ANALYSIS

Single-folding DWBA calculations (as described in Refs. [9,10,16]) were carried out with PTOLEMY [17]. Optical model parameters obtained for 240 MeV α scattering on ^{90}Zr [18] were used and are shown in TABLE I. In addition to the experimental uncertainties indicated in the tables for the EWSR, a variation of optical parameters has been shown to change the DWBA cross-sections [18] by 10-15%.

TABLE I. Optical Model potential and Fermi mass density parameters used in DWBA calculations for ^{94}Mo are shown, r_{c0} is the Coulomb radius parameter.

V (MeV)	W (MeV)	r_i (fm)	a_i (fm)	r_{c0}	c	a
40.2	40.9	0.786	1.242	.960	5.0264	.515

Calculations were performed with a Fermi mass distribution, $\rho(r) = \rho_0 \left[1 + e^{\frac{r-c}{a}}\right]^{-1}$, with c and a shown in Table I [19]. The calculations for the transition densities, sum rules, and DWBA calculations were discussed thoroughly in Refs. [9,10,16,20].

A continuum of events consisting of various reactions such as multipole excitation, multistep excitation, pickup-breakup, and knock-out reactions as well as possibly some background from slit scattering is present in the data. In the analysis of the data, this continuum is represented by a straight line at high excitation joined to a Fermi shape at low-excitation to model the particle decay threshold. The inelastic α spectra obtained at several angles are each divided into a peak and continuum.

The peak and continuum cross-sections are then divided into bins by excitation energy. To obtain the multipole components for each bin, the experimental angular distributions of the peak and continuum cross-sections are compared to the single-folding DWBA calculations done with PTOLEMY, and then the strengths of the isoscalar L=0-4 contributions are varied in order to minimize χ^2. The Isovector Giant Dipole Resonance (IVGDR) contributions are calculated and held fixed in the fits. The experimental and calculated angular distributions are illustrated in Figure 2 for selected energy bins for the GR peak and continuum. The uncertainty for each

multipole is determined by incrementing or decrementing the strength of that multipole, adjusting the strengths of other multipoles by fitting to the data, and continuing until the new χ^2 is 1 unit larger than the χ^2 from the best fit.

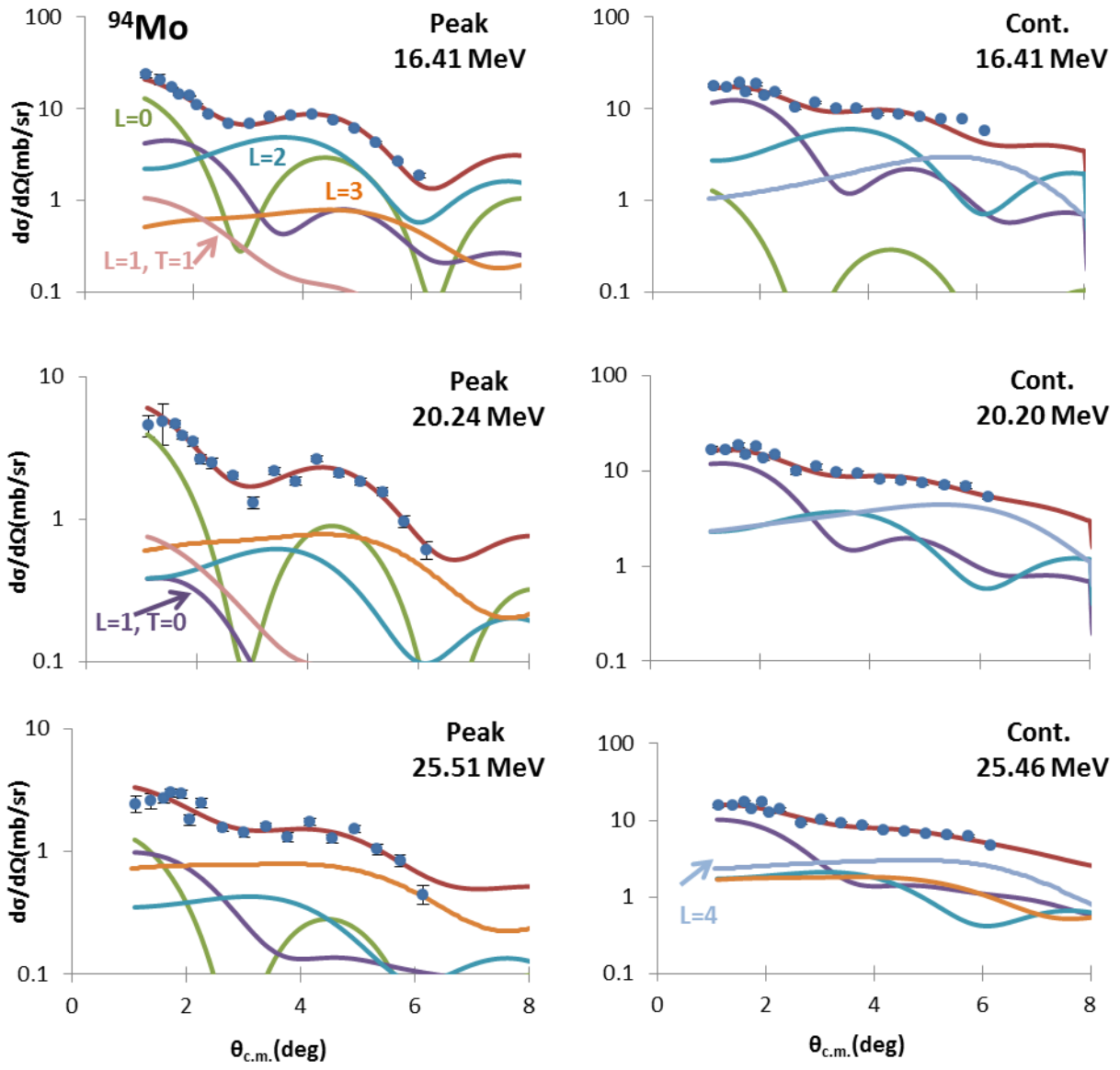

FIG. 2. ^{94}Mo differential cross sections for three excitation ranges of the GR peak and the continuum are plotted vs. center-of-mass scattering angle. Each bin is 480 keV wide and the average energies for each bin are shown. The lines through the data points indicate the multipole fits. The contributions of each multipole are shown. The statistical errors are shown but are mostly smaller than the data points.

Analyses are done several times using different assumptions about the continuum in order to estimate the uncertainties due to the choice of continuum. Typical choices for the continuum can be seen in Figure 1. For purposes of estimating the uncertainties, the continuum could have a linear slope at high excitation that does not quite match the experimental data, could be lowered so that it is always below the data, could have a different low energy cutoff and slope, or can have slope and or amplitude which is altered at selected angles.

These separate analyses are then combined into an average distribution. Errors were calculated by adding the errors from the multipole fits (30-60% of the total uncertainty) in quadrature with the standard deviations between the different fits (generally between 1-4% of the total uncertainty) and the systematic experimental uncertainty.

IV. DESCRIPTION OF MICROSCOPIC CALCULATIONS

Microscopic mean-field based Random Phase Approximation (RPA) theory provides a description of collective states in nuclei [3,21]. A description of the spherical HF-based RPA calculations of the strength functions and centroid energies of the isoscalar (T=0) giant resonances in nuclei can be found in Ref. [7] and is summarized below.

The strength or response function can be obtained from the RPA states $|n\rangle$ with corresponding energy E_n:

$$S(E) = \sum_n |\langle 0|F|n\rangle^2 |\delta(E - E_n), \quad (2)$$

where F is the single particle scattering operator $F = \sum f(i)$. The ISGMR energies ($m_k = \int E^k S(E) dE$) are given by:

$$E_{con} = \sqrt{\frac{m_1}{m_{-1}}} \qquad E_{cen} = \frac{m_1}{m_0} \qquad E_{scal} = \sqrt{\frac{m_3}{m_1}} \tag{3}$$

where, E_{con} is the constrained energy, E_{cen} is the centroid energy, and E_{scal} is the scaling model energy. The Energy Weighted Sum Rule (EWSR), m_1, is calculated using the Hartree-Fock ground state wave function.

The fully self-consistent mean field calculation of the response function uses an effective two-nucleon interaction which is obtained from a fit to the ground states properties of nuclei. The effective interaction determines the HF mean-field. The RPA calculation includes all of the components of the two-body interaction using a large configuration space and was done using the numerical approach of Refs. [13,22]. The calculations of the strength functions and centroid energies of the isoscalar (T=0) giant resonances in the nuclei were done using an occupation number approximation for the single particle orbits of open shell nuclei. For the single-particle scattering operator $F = \sum_i f(r_i) Y_{L0}$ we used $f(r) = r^2$ for the monopole (L=0) and quadrupole (L=2), $f(r) = r^3$ for the Octopole (L=3), and $f(r) = r^3 - \frac{5}{3}\langle r^2 \rangle r$ was used for the dipole (L=1). The form of the dipole scattering operator takes into account the contribution from spurious states [23,24]. The KDE0v1 Skyrme-type effective interaction was used. In an external test of 240 Skyrme-type effective interactions [25,26], the KDE0v1 was the only one to pass constraints relating to experimental data on properties of nuclear matter and nuclei.The appropriate experimental excitation energy ranges were used: 9-40 MeV for the ISGMR and ISGQR, 9-20 MeV for the low-component of the ISGDR, 20-36 MeV for the high-component of

the ISGDR, and 14-40 MeV for the HEOR. The calculated distributions are shown superimposed on the experimental results in Figure 3. The smearing width (Γ) for the calculated distributions for the E0-E3 multipoles are shown in Table II and are FWHM. The smearing widths were chosen so that the visual rendering of the calculation would provide a good comparison with the experimental strength distribution. The energy moments are included in Tables III and V. The theoretical strengths are calculated over a range of 0 to 100 MeV and contain 100% of the EWSR for E0-E3.

TABLE II. The Lorentzian smearing width (Γ) for the calculated distributions are shown.

	E0	E1	E2	E3
Γ (MeV)	6.5	5.0	10.0	13.0

V. DISCUSSION

The E0-E3 multipole distributions obtained for ^{94}Mo are shown in Figure 3. Two peak fits are shown for the E0 and E1 distributions, and a single Gaussian fit is shown for E2 and E3. The parameters for these fits and for the moment ratios (m_1/m_0 and $\sqrt{(m_3/m_1)}$) are shown in

TABLE III.

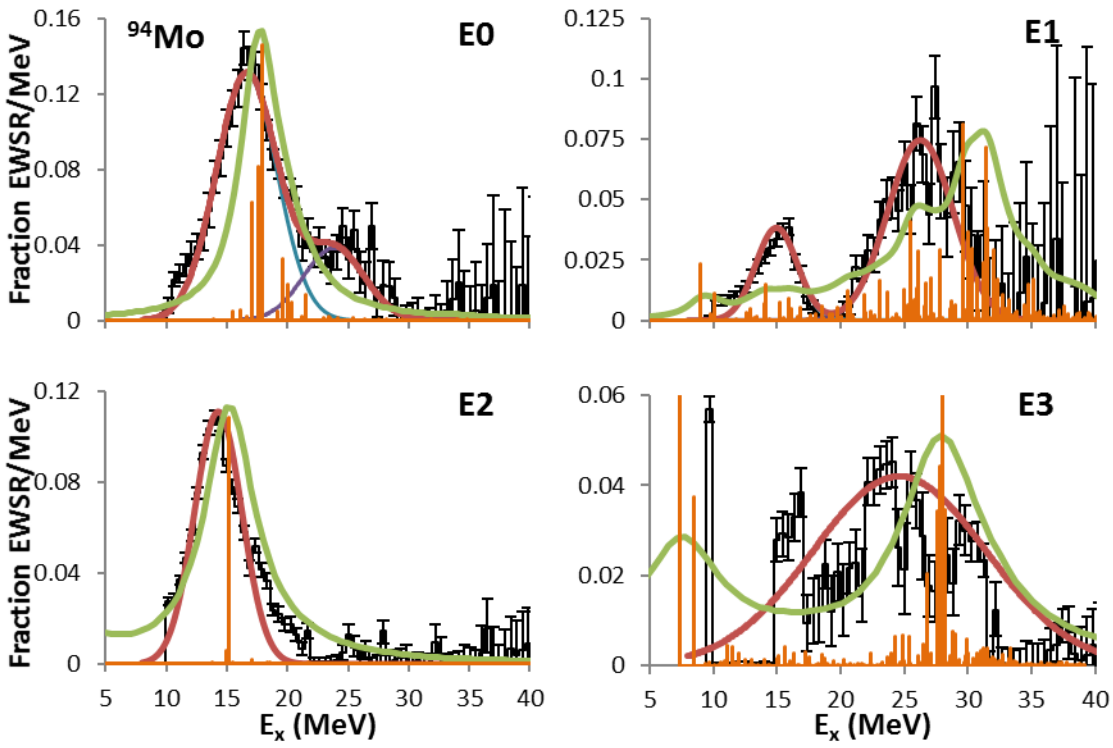

FIG. 3. Strength distributions obtained for ^{94}Mo are shown by the histograms. Error bars represent the uncertainty based on the fitting of the angular distributions and different choices for the continuum, as described in the text. Gaussian fits to the E0 and E1 distributions for the individual peaks (blue and purple) and their sum (red) are shown. The green lines are the strength distributions obtained with the HF-RPA calculations using the KDE0v1 interaction, smeared using the widths in Table II to more closely represent the data as discussed in the text.

The orange lines are the HF-RPA strength distributions without smearing and with the strength scaled to fit on the figure.

TABLE III. Parameters for energy moments obtained for isoscalar multipoles in ^{94}Mo are shown. The moments from the KDE0v1 calculation results are over the experimental energy range $9 \leq E_x \leq 40$ MeV.

	Moments				
	$E0$		$E1$	$E2$	E3
	Exp.	KDE0v1			
m_1 (Frac. EWSR)	$1.12 \pm^{.19}_{.12}$	.95	$0.83 \pm^{.35}_{.20}$	$0.77 \pm^{.11}_{.10}$	$.45 \pm .10$
m_1/m_0(MeV)	$17.57 \pm^{1.14}_{.30}$	18.06	$24.57 \pm^{3.41}_{1.59}$	$16.12 \pm^{.66}_{.39}$	$21.10 \pm^{.31}_{.17}$
rms width (MeV)	$5.68 \pm^{5.53}_{1.93}$	4.40	$8.02 \pm^{3.89}_{1.81}$	$7.61 \pm^{1.74}_{1.04}$	$6.64 \pm^{.53}_{.30}$
$\sqrt{m_3/m_1}$ (MeV)	$19.62 \pm^{3.54}_{1.15}$	19.39	$28.20 \pm^{4.61}_{2.11}$	$19.56 \pm^{1.92}_{1.12}$	$24.03 \pm^{.73}_{.28}$
$\sqrt{m_1/m_{-1}}$ (MeV)	$17.06 \pm^{.75}_{.19}$	17.67	$23.09 \pm^{2.84}_{1.31}$	$15.48 \pm^{.44}_{.26}$	$19.84 \pm^{.23}_{.17}$

TABLE IV. Parameters obtained for Gaussian fits for isoscalar multipoles in ^{94}Mo are shown.

	Gaussian fits

	$E0$ peak 1	E0 peak 2	$E2$
Centroids (MeV)	$16.51\pm^{.19}_{.21}$	$23.59\pm^{.78}_{.76}$	$14.55 \pm .13$
FWHM (MeV)	$5.73\pm^{.39}_{.36}$	$5.87\pm^{1.06}_{1.14}$	$5.28 \pm .17$
Frac. EWSR	0.82±.06	0.21±.05	0.59±.03
		Gaussian fits	
	$E1$ Low Peak	$E1$ High Peak	E3
Centroids (MeV)	$15.07\pm^{.22}_{.19}$	$26.50\pm^{.44}_{.42}$	24.60±.46
FWHM (MeV)	$3.19\pm^{.36}_{.22}$	$5.99\pm^{.45}_{.49}$	$9.24\pm^{.53}_{.50}$
Frac. EWSR	0.12±.02	0.45±.05	0.39±.03

TABLE V. Parameters obtained for energy moments from the KDE0v1 calculation are shown. The results are over the experimental energy ranges (E1 low range: 9≤Ex≤20 MeV, E1 high range: 20≤Ex≤40 MeV, E2: 9≤Ex≤40 MeV, and E3: 14≤Ex≤40 MeV)

	KDE0v1			
	$E1$ Low Range	$E1$ High Range	E2	E3
m_1/m_0 (MeV)	14.29	29.05	16.54	25.98
rms width (MeV)	3.31	4.49	5.05	5.63
m_1 (Frac. EWSR)	0.13	0.77	0.86	0.64

A. E0 Strength

In the E0 strength distribution, 112^{+19}_{-12}% of the sum rule was identified in the energy range analyzed, $9 \leq E_x \leq 40$ MeV. As in other A≈90 nuclei [6--8], the strength is separated into high and low energy components. The low-energy component is fit well with a Gaussian centered at 16.51 MeV. This peak contains about 82% of the EWSR. The high-energy component is at 23.59 MeV and contains approximately 21% of the EWSR. The energies and strengths of the components follow the general trend seen for the other Mo isotopes studied in Refs. [6,7]. The energies obtained for the 4 Mo isotopes from Refs. [6,7] and for ^{94}Mo from the two peak fits are plotted versus A in Figure 4. Lines representing $74/A^{\frac{1}{3}}$ and $109/A^{\frac{1}{3}}$ are shown as a reference on the low and high plots. The low energy peak is possibly decreasing faster than $A^{-1/3}$, while the high energy peak shows no systematic change in energy. As was observed in the other Mo isotopes [6,7], the results of the HF-RPA calculation for the E0 strength calculation show a single, slightly asymmetrical peak concentrated in a narrow band just above the narrow peak in the data. Although the distributions are not in agreement, the centroid, scaled, and constrained energy moments are in agreement within the errors.

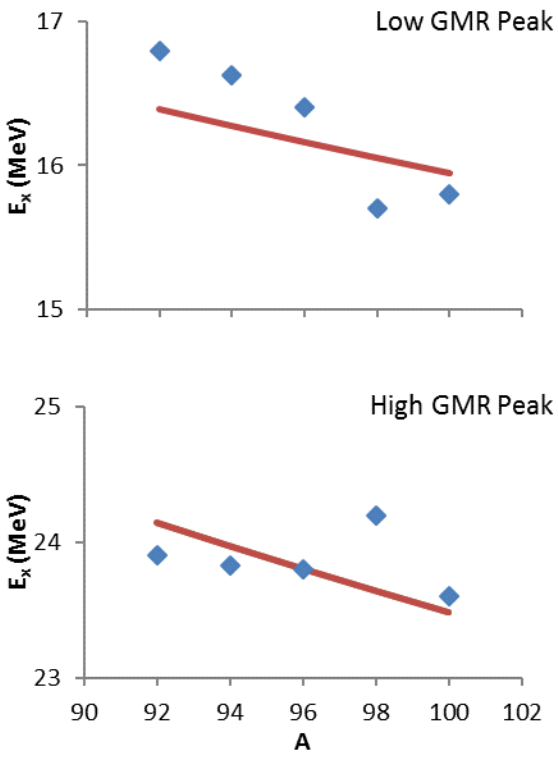

FIG. 4. The centroids of the Gaussians obtained from the fits to the E0 distributions for the Mo isotopes are plotted vs. A. The (red) lines show $74A^{-1/3}$ and $109A^{-1/3}$ in the upper and lower plots respectively.

B. E1 Strength

Much of the expected E1 EWSR ($83\pm^{35}_{20}$%) was identified in the range 9-40 MeV. The strength is divided into $1\hbar\omega$ and $3\hbar\omega$ [27--29] components. The high energy component is the compression mode, and its energy is related to K_A. The low energy component is mostly in the range $9\leq E_x\leq 20$ MeV, and the high energy component is mostly in the range $20\leq E_x\leq 36$ MeV [7]. The high and low peaks are fit well with Gaussians. The low energy component is at $15.07\pm^{.22}_{.19}$ MeV and contains 12% of the EWSR, and the high energy component is at $26.50\pm^{.44}_{.42}$ MeV and contains 45% of the EWSR. The sum of the strength in these two components is less than the 83% observed over the 9 – 40 MeV range. In the E1 strength distribution for energies above 30 MeV (Figure 3), the strength has large error bars which extend to the x-axis, and in this region the strength may effectively be zero. The results of the HF-RPA calculations for the E1 strength (broadened with a Lorentzian shape with Γ = 5.0 MeV) are shown superimposed on the data in Figure 3. The calculated strength is in a broad peak with some strength at low excitation and indications of several components and structure at ≈27 and 32 MeV. The strength rises to a maximum near 30 MeV, roughly 4 MeV greater than the high peak from the experimental strength, and then tails past 40 MeV. In the low energy range ($9\leq E_x\leq 20$ MeV) there is a weak peak near the experimental one and also another one below it. The calculation and the data do not agree, but the amount of strength predicted in the low energy range is nearly the same as the experimental value obtained from the Gaussian fit of the low peak. In the high energy range ($20\leq E_x\leq 40$ MeV), the calculation for the peak position is greater than the experimental one by ≈2 MeV and predicts more strength than identified in the experimental data. In Figure 5, the centroids of the Gaussian fit to the low and high energy peaks and the strength in the low and high peaks for the isotopes from Ref. [7] and for ^{94}Mo is plotted vs A. For the Mo isotopes, the

calculated positions of the low and high energy peaks tend to not be in agreement with the experimental position.

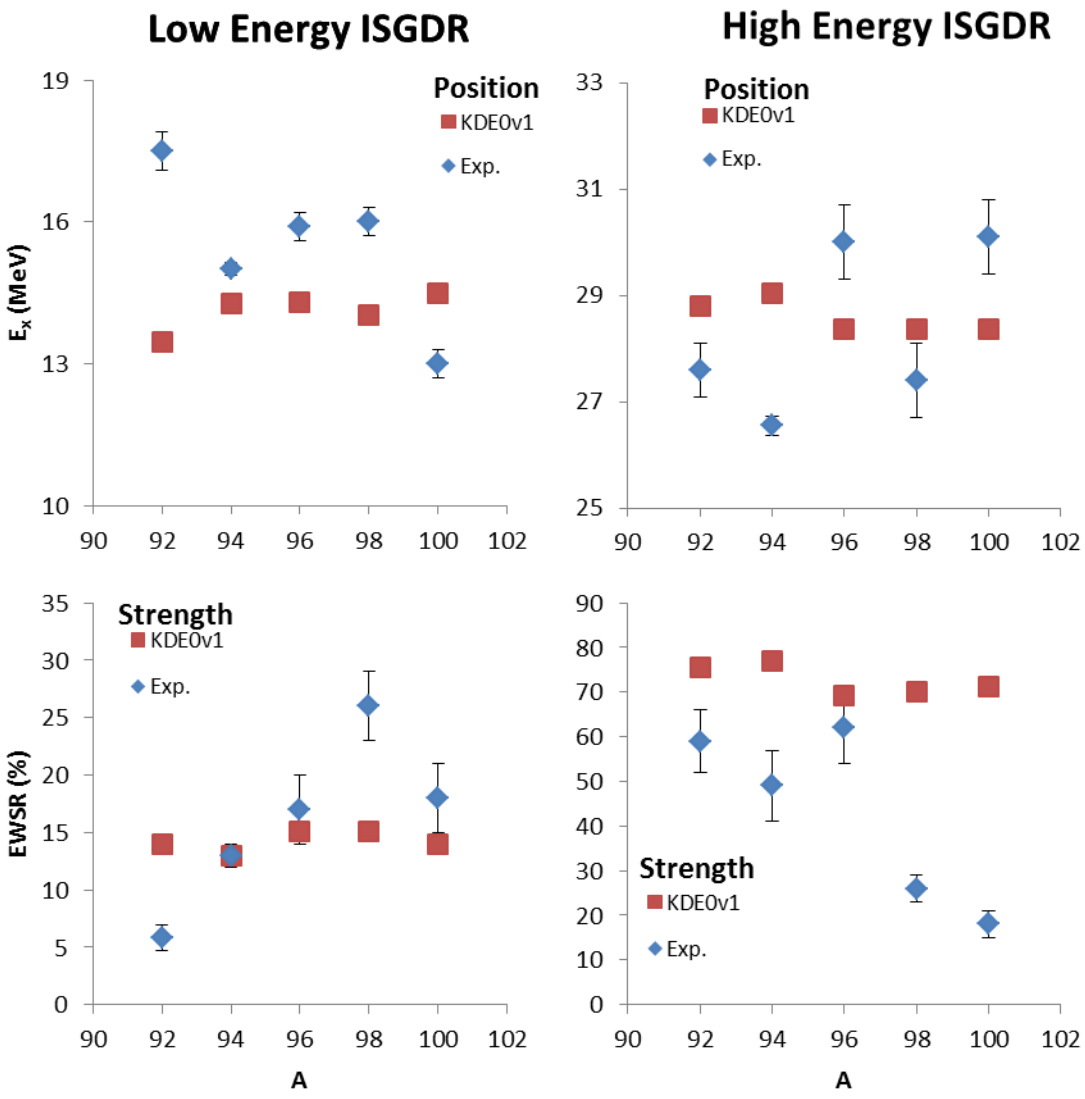

FIG. 5. The centroids of the Gaussian fits to the low and high energy peaks in the ISGDR distributions for each of the Mo isotopes from Ref. [7] and ^{94}Mo from this work are plotted vs. A in the top panels. The strength in the low and high peak is plotted in the lower panels.

C. E2 Strength

The E2 peak is located at (m_1/m_0) 14.56±.09 MeV and 61±9% of the E2 EWSR was identified. The peak was fitted with a Gaussian and m_1/m_0, RMS width, and the Gaussian parameters are given in

Table IV. The Gaussian energy is approximately 1.5 MeV less than m_1/m_0 because of the inclusion of the apparently random strength at high excitation in the calculation of the energy moments. In the Mo isotopes studied in Ref. [7], the E2 strength distribution was slightly asymmetric on the low energy side. Moalem *et al.* [4] measured the GQR in ^{94}Mo with inelastic scattering of 110 MeV ^{3}He. Our result for %EWSR, Gaussian energy, and width agree within the errors with their work. Figure 6 compares the Gaussian centroid energy of the GQR in the Mo isotopes obtained from the four experiments [4,5,7], the GQR measurement of ^{92}Mo with inelastic scattering of 120 MeV α particles by Duhamel *et al.* [5], and the m_1/m_0 obtained from the calculation with the KDE0v1 interaction. The calculated distribution shows a peak that is located at a higher energy by approximately 1 MeV, but it does show a similar amount of tailing on the high excitation side.

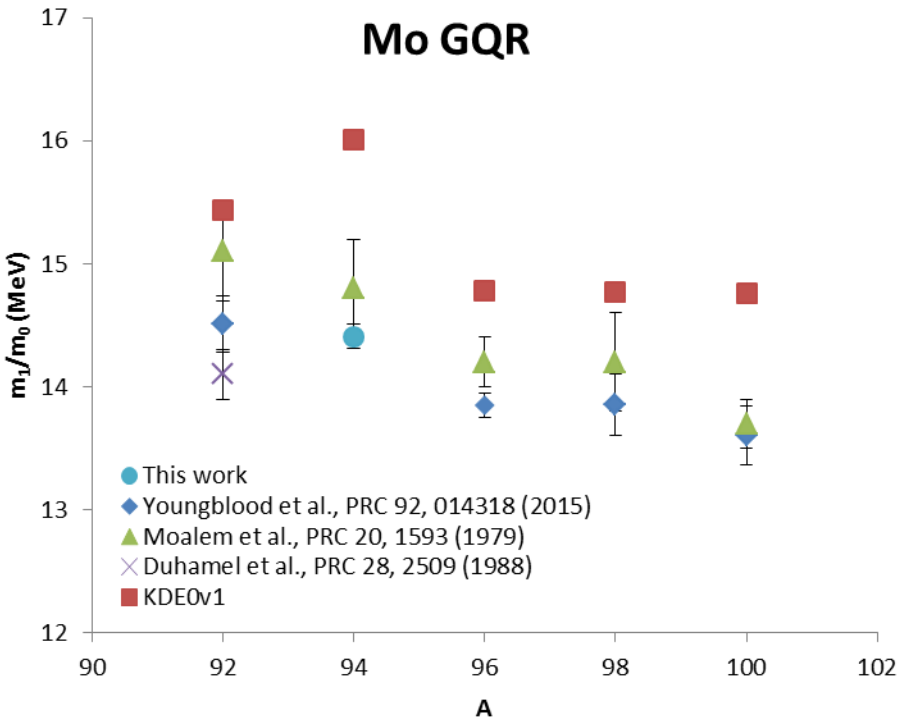

FIG. 6. The centroid of the Gaussian fit to the E2 strength in each of the Mo isotopes from Ref. [7] (blue diamonds) and ^{94}Mo from this work (light blue circle) is plotted vs. A.

D. E3 Strength

In the Harmonic Oscillator Shell Model description of the Giant Resonances, the E3 resonance is split into a 1$\hbar\omega$ low energy octupole (LEOR) containing 25% of the E3 EWSR and 3$\hbar\omega$ high energy octupole (HEOR) containing 75% of the EWSR [30]. Coupling these modes with the octupole/octupole residual reaction gives an LEOR with approximately 35% of the EWSR and HEOR with 65% EWSR [30]. The low-energy cutoff for the measured data lies in the middle of the higher region of the LEOR. The HF-RPA calculation with KDE0v1 interaction puts the LEOR at about 8 MeV, which is below the 9 MeV cutoff. The HEOR is predicted to be located at about 29 MeV. The experimental strength for the HEOR is in a broad peak centered at 24.6

MeV and contains 39% of the E3 EWSR. The calculated energy is 25.98 MeV. As was noted in Ref [7] , the calculated energies for the HEOR are sensitive to the effective mass. Using a larger effective mass would lower the predicted energy.

VI. SUMMARY

We have obtained distributions for isoscalar E0, E1, E2, and E3 strength in ^{94}Mo and compared these to spherical Hartree-Fock-RPA calculations using the KDE0v1 Skyrme type interaction. The E0 strength has a high energy tail similar to that in the A≠92 Mo nuclei which is not present in heavier nuclei. The source of this tail is not understood. The position of the high energy part of the isoscalar dipole is about 2.5 MeV below that from the HF-RPA calculation. Position, strength and width of the E2 distributions agree within errors with those obtained by Moalem *et al.*, but are ≈1 MeV below those obtained with the HF-RPA calculations. The HEOR strength lies in a broad peak centered at 24.6 MeV, approximately 2 MeV below that obtained with the HF-RPA calculations.

Microscopic calculations beyond the mean-field approximation, which include nuclear structure effects, may be necessary to obtain the correct energies and strength distributions. Additionally, using microscopic transition densities in analyses of the experimental cross-section data may improve agreement between experiment and theory.

ACKNOWLEDGMENTS

This work was supported, in part, by the U.S. Department of Energy under Grant No. DE-FG03-93ER40773.

REFERENCES

[1] J. P. Blaizot, Phys. Rep. **64**, 171 (1980).

[2] J. Treiner, H. Krivine, O. Bohigas, and J. Martorell, Nucl. Phys. A **371**, 253 (1981).

[3] S. Shlomo, V. M. Kolomietz, and G. Colò, Eur. Phys. J. A **30**, 23 (2006).

[4] A. Moalem, Y. Gaillard, A. Bemolle, M. Buenerd, J. Chauvin, G. Duhamel, D. Lebrun, P. Martin, G. Perrin, and P. De Saintignon, Phys. Rev. C **20**, 1593 (1979).

[5] G. Duhamel, M. Buenerd, P. De Saintignon, J. Chauvin, D. Lebrun, P. Martin, and G. Perrin, Phys. Rev. C **38**, 2509 (1988).

[6] D. H. Youngblood, Y. -W. Lui, J. Button, M. R. Anders, M. L. Gorelik, M. H. Urin, and S. Shlomo, Phys. Rev. C **88**, 021301 (2013).

[7] D. H. Youngblood, Y. -W. Lui, J. Button, G. Bonasera, and S. Shlomo, Phys. Rev. C **92**, 014318 (2015).

[8] Krishichayan, Y. -W. Lui, J. Button, D. H. Youngblood, G. Bonasera, and S. Shlomo, Phys. Rev. C **92**, 044323 (2015).

[9] D. H. Youngblood, Y. -W. Lui, and H. L. Clark, Phys. Rev. C **65**, 034302 (2002).

[10] D. H. Youngblood, Y. -W. Lui, and H. L. Clark, Phys. Rev. C **63**, 067301 (2001).

[11] D. H. Youngblood, Y. -W. Lui, and H. L. Clark, Phys. Rev. C **61**, 067307 (2000).

[12] D. H. Youngblood, Y. -W. Lui, and H. L. Clark, Phys. Rev. C **60**, 014304 (1999).

[13] P. - G. Reinhardt, Ann. Phys. (Leipzig) **1**, 632 (1992).

[14] B. K. Agrawal, S. Shlomo, and V. K. Au, Phys. Rev. C **72**, 014310 (2005).

[15] K. van der Borg, M. N. Harakeh, and A. van der Woude, Nucl. Phys. A. **265**, 243 (1981).

[16] G. R. Satchler and D. T. Khoa, Phys. Rev. C **55**, 285 (1997).

[17] M. Rhoades-Brown, S. Pieper, and M. Macfarlane, *in Argonne National Laboratory Report* (Argonne National Laboratory, Argonne, 1978).

[18] Krishichayan, X. Chen, Y. -W Lui, J. Button, and D. H. Youngblood, Physical Review C **81**, 044612 (2010).

[19] G. Fricke, C. Bernhardt, K. Heilig, L. A. Schaller, L. Schellenberg, E. B. Shera, and C. W. De Jager, At. Data Nucl. Data Tables **60**, 177 (1995).

[20] H. L. Clark, Y. -W. Lui, and D. H. Youngblood, Phys. Rev. C **57**, 2887 (1998).

[21] A. Bohr and B. R. Mottelson, *Nuclear Structure* (W.A. Benjamin, New York, 1975), Vol. 2.

[22] T. Sil, S. Shlomo, B. Agrawal, and P. Reinhard, Phys. Rev. C **73**, 034316 (2006).

[23] S. Shlomo and A. Sanzhur, Phys. Rev. C **65**, 044310 (2002).

[24] B. K. Agrawal, S. Shlomo, and A. Sanzhur, Phys. Rev. C **67**, 034314 (2003).

[25] P. Stevenson, P. Goddard, J. Stone, and M. Dutra, arXiv preprint arXiv:1210.1592 (2012).

[26] M. Dutra, O. Lourenço, J. S. Martins, A. Delfino, J. R. Stone, and P. Stevenson, Physical Review C **85**, 035201 (2012).

[27] H. L. Clark, Y. -W. Lui, and D. H. Youngblood, Phys. Rev. C **63**, 031301(R) (2001).

[28] G. Colo, N. van Giai, P. F. Bortingon, and M. R. Quaglia, Phys. Lett. B **485**, 362 (2000).

[29] D. Vretenar, A. Wandelt, and P. Ring, Phys. Lett. B **487**, 334 (2000).

[30] J. M. Moss, D. H. Youngblood, C. M. Rozsa, D. R. Brown, and J. D. Bronson, Phys. Rev. Lett. **37**, 816 (1976).